



**HAL**  
open science

# Influence of Milling Tool and Prosthetic Materials on Roughness of the Dental CAD CAM Prostheses in End Milling Mode

Nicolas Lebon, Laurent Pierre Tapie, Elsa Vennat

► **To cite this version:**

Nicolas Lebon, Laurent Pierre Tapie, Elsa Vennat. Influence of Milling Tool and Prosthetic Materials on Roughness of the Dental CAD CAM Prostheses in End Milling Mode. Applied Sciences, 2020, 10 (7), pp.2238. 10.3390/app10072238 . hal-02554134

**HAL Id: hal-02554134**

**<https://hal.science/hal-02554134>**

Submitted on 13 Jul 2020

**HAL** is a multi-disciplinary open access archive for the deposit and dissemination of scientific research documents, whether they are published or not. The documents may come from teaching and research institutions in France or abroad, or from public or private research centers.

L'archive ouverte pluridisciplinaire **HAL**, est destinée au dépôt et à la diffusion de documents scientifiques de niveau recherche, publiés ou non, émanant des établissements d'enseignement et de recherche français ou étrangers, des laboratoires publics ou privés.



Distributed under a Creative Commons Attribution 4.0 International License

Article

# Influence of Milling Tool and Prosthetic Materials on Roughness of the Dental CAD CAM Prosthesis in End Milling Mode

Nicolas Lebon <sup>1,\*</sup> , Laurent Tapie <sup>1</sup> and Elsa Vennat <sup>2</sup>

<sup>1</sup> Department of Biomaterials, URB2i-UR 4462, Faculty of Dental Surgery, Paris and Sorbonne Paris Nord Universities, 93430 Paris, France; laurent.tapie@univ-paris13.fr

<sup>2</sup> Soil, Structures and Materials Mechanics Laboratory UMR CNRS 8579, Centrale-Supelec Paris, Paris-Saclay University, 91190 Gif-sur-Yvette, France; elsa.vennat@ecp.fr

\* Correspondence: lebon@univ-paris13.fr; Tel.: +33-(1)-58-07-67-85

Received: 27 February 2020; Accepted: 21 March 2020; Published: 25 March 2020



**Abstract:** Dental prostheses are machined by computer-aided design and manufacturing (CAD/CAM) tools. The integrity of the surface obtained, which must be suitable to meet expected clinical requirements is influenced by the milling parameters programmed. The integrity of the occlusal prosthesis surface obtained by the end milling mode, that is milling with a diamond rotary cutting tip, plays a major role in the clinical requirements desired. This study aims to investigate the impact of the tool-biomaterial couple in the CAD/CAM end milling mode on surface integrity (through roughness). Two CAD/CAM tools and four CAD/CAM biomaterials, both combined to four feed rates are tested. The surface roughness ( $R_a$ ,  $R_t$ ,  $R_z$ ,  $S_a$ ,  $S_q$ , and  $S_z$ ) is observed for each couple. Finally, pairwise comparisons (Kruskal-Wallis test) of tool-biomaterial couples are performed. The results indicate that all the machined surfaces reveal isotropic surface topology. The roughness depends on the hardness of the biomaterial and not on the feed rate. The statistical tests reveal a significant difference in roughness depending on the tool used. To conclude, when milling the functional occlusal shape, biomaterial hardness and the tool used are key factors for achieving a given roughness consistent with clinical requirements.

**Keywords:** CAD CAM; milling; roughness; dental materials; surface integrity

## 1. Introduction

Contemporary dental Computer Aided Design/Computer Aided Manufacturing (CAD/CAM) technology is used to manufacture dental prostheses. According to recent studies reports [1–3], the global market for Dental CAD/CAM is booming and expected to achieve prominence by 2024–2027, with an expected growth rate of about 5.6% to 8.1% per year.

However, the dental CAD/CAM process requires several steps to produce a prosthesis, with the last step the milling process performed with a Numerical Controlled (NC) milling machine. This NC milling step plays a crucial role as it generates a characteristic “signature” on the prosthesis shape called surface integrity (SI), not sufficiently understood at present in restorative dentistry [4]. These SI properties (roughness, hardness, marginal chipping, porosity, internal stress, etc.) of the milled prosthesis are mainly affected by the milling process [5]. In addition, several requirements of the prosthesis surface such as aesthetics, biological response (dental plaque retaining) and mechanical behavior (micromechanical retention of the cement or/and adhesion on the intaglio surface) and restoration lifetime are highly dependent on residual roughness after CAD/CAM milling [6–13].

Prosthetic surface roughness is a crucial parameter and a specific roughness can be manufactured for each clinical requirement. For example, restoration lifetime, aesthetics and biological response

require a minimal surface roughness currently ensured by polishing after CAD/CAM [14]. Such surface roughness should be obtained directly after milling by optimizing milling parameters. On the contrary, the surface to be bonded must be sufficiently rough to ensure good bonding [15].

To fulfill these clinical requirements, several classes of biomaterials are available on the marketplace, such as ceramics, composite resins and PICN (Polymer-Infiltrated Ceramic-Network) [16–19]. These biomaterial classes differ considerably in their mechanical, chemical and machinability properties. However, few data on their properties after milling are provided in the literature [20,21]. This article focuses on the properties of biomaterial SI after milling. In addition, biomaterial SI properties also depend on the tool-biomaterial couple used [22]. The tool-biomaterial couple is composed of the tool (diamond rotary cutting instrument) used, the milled biomaterial, and the milling parameters (such as feed rate) programmed [23,24]. To the best of our knowledge the interactions between the tool-biomaterial couple and SI, in dentistry, have not yet been studied. The aim of this study is to assess these interactions in the end milling mode (use of the tool tip for milling). The SI properties are mainly described through roughness parameters [25–28].

The first null hypothesis of this study is that roughness does not vary depending on the tool-biomaterial couple while the second null hypothesis is that roughness does not vary as a function of the feed rate.

## 2. Materials and Methods

Four typical machinable biomaterials and two marketed tools are studied. The milling conditions are as close as possible to those used in a daily practice. After milling, surface topology and six roughness amplitude parameters are measured and analysed for each sample.

### 2.1. Tool-Biomaterial Couples

To be as representative as possible of the dental marketplace, four machinable biomaterials (two ceramic, one composite and one PICN) and two commercial CAD/CAM tools are used in this study (Tables 1 and 2). The two tool geometries are described in Figure 1. The eight practicable tool-biomaterial couples investigated are presented in Table 3.

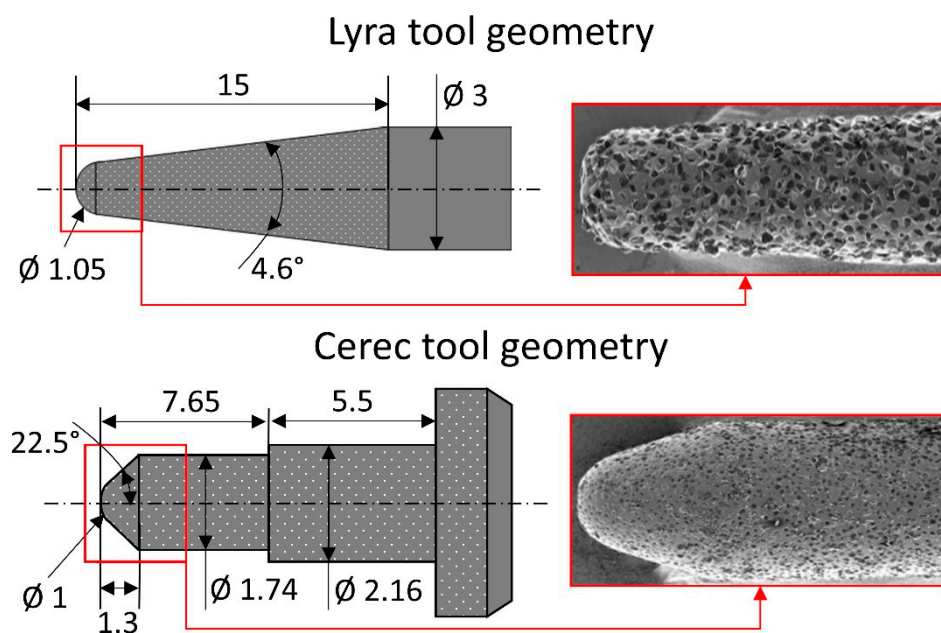


**Figure 1.** Geometry of the two tools used in the study (all lengths and diameters in mm).

**Table 1.** Biomaterials used in the study.

Biomaterials	Manufacturer	Class of Biomaterial	Lot Number	Vickers Hardness	Code
Celtra Duo	Dentsply Sirona	Zirconia-reinforced lithium silicate glass ceramics	18016461	737 Hv <sup>(1)</sup> (Hard)	CD
Mark II	VITA Zahnfabrik	Fine particle feldspar ceramic resin	43660	640 Hv <sup>(2)</sup> (Hard)	MK
Lava Ultimate	3M ESPE	Nano-ceramic resin composite	N606702	107.3 Hv <sup>(3)</sup> (Soft)	LU
Enamic	VITA Zahnfabrik	Hybrid (resin-infiltrated ceramic networks)	42010	254.9 Hv <sup>(4)</sup> (Medium)	EN

(1) from our laboratory tests. (2) from the manufacturer’s web site pdf file. (3) from our laboratory tests. (4) from the manufacturer’s web site pdf file. (1 Hv = 0.009807 GPa). (4) from the manufacturer’s web site pdf file. (1 Hv = 0.009807 GPa).

**Table 2.** Tools used in the study. (SD: Standard Deviation).

Tool	Manufacturer	Diamond Grain Size	Code
Conical bur Ø1.05 mm	Lyra-GACD SASU	78 µm (SD = 17.5 µm)	LY
Cerec cylinder pointed bur 12S	Sirona Dental Systems	43.5 µm (SD = 10 µm)	CER

**Table 3.** Tool-biomaterial couples codes.

		Biomaterials			
		MK	LU	EN	CD
Tools	LY	MKLY	LULY	ENLY	CDLY
	CER	MKCER	LUCER	ENCER	CDCER

**2.2. Milling Conditions**

A four axis (X, Y, Z, A) milling center (Lyra-GACD prototype) is used to mill all the samples. The experiments are performed in end milling mode at a constant spindle speed of 60,000 RPM. End milling mode is when the end tip (not the flank) of the tool is used to mill the surface (Figure 2). The milling center is warmed up before milling, if necessary (axis and spindle thermal stabilization). During milling, a coolant is sprayed on to the tool-biomaterial contact area at a constant coolant flow rate.

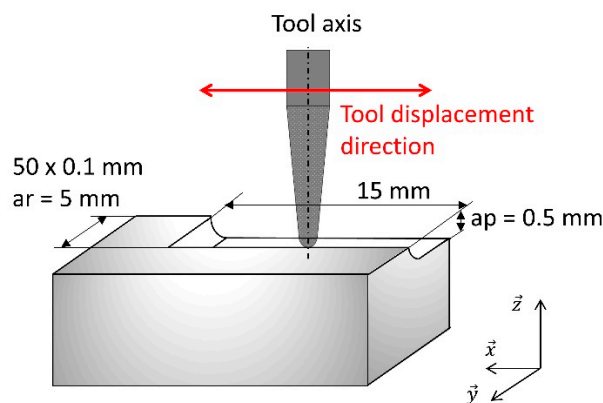


**Figure 2.** End milling mode mapping.

The influence of the feed rate on the surface roughness with the eight practicable couples is investigated at four different feed rates (1000-2000-3000-4800 mm/min). The feed rate is the relative displacement speed between the tool and the workpiece. Therefore, thirty-two experiments are necessary (Figure 3). These four feed rates are tested on the same biomaterial CAD/CAM raw block (one feed rate per side). A new tool is used for each new biomaterial raw block. For each experiment, a planar area ( $5 \times 15 \text{ mm}^2$ ) is milled on each side of the CAD/CAM block (Figure 3, Step A). The size of the planar machined surface is suitable with the raw dimensions of the CAD/CAM block and allows the topology and 3D roughness to be measured correctly, freeing it from unusable areas (CNC acceleration/deceleration areas). The axial ( $a_p$ ) and radial ( $a_r$ ) depths are 0.5 mm and 0.1 mm respectively. To sweep  $5 \times 15 \text{ mm}^2$  with a radial depth of 0.1 mm each tool moves back and forth fifty times. The total path length is 750 mm ( $=50 \times 15 \text{ mm}$ ) per feed rate. The total milled volume (chip volume) per tool is  $150 \text{ mm}^3$  ( $=15 \text{ mm} \times 5 \text{ mm} \times 0.5 \text{ mm} \times 4$ ). All the dimensions are reported in Figure 2.

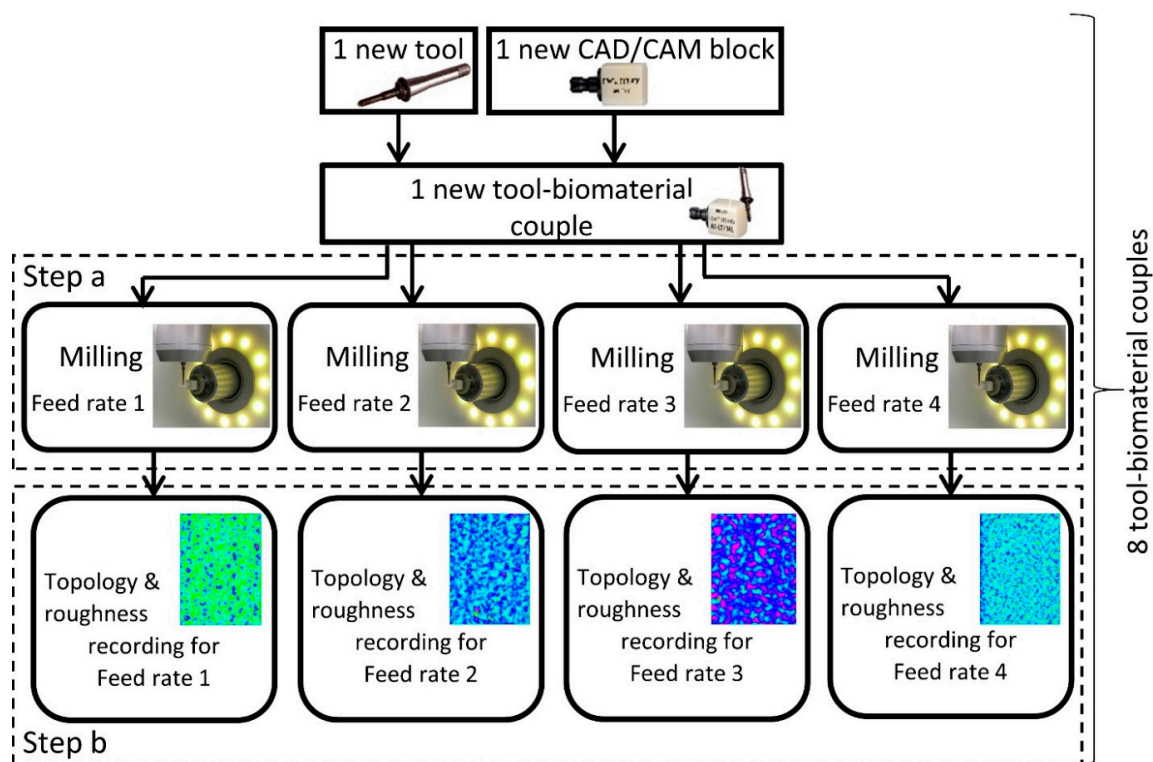


**Figure 3.** Diagram of experiment protocol.

### 2.3. Surface Topography Recording

The surface topography is recorded according to the diagram presented in Figure 3. Each milled surface topography is optically recorded in 3D (Figure 3, Step B) with a focal variation device (Bruker Alicona, Infinite Focus). Focus variation is a method that allows the measurement of areal surface topography using optics with limited vertical scanning and depths of field. Depth measurement by focus variation is obtained by searching the best focus position of an optical element pointing to a sample. This position in focus field is related to a distance from the sample (depth). This operating principle is in line with the ISO standard 25178 for classifying surface texture method. Two planar surfaces ( $0.8 \times 1 \text{ mm}^2$ ) per sample are recorded in the middle of each milled surface with a vertical resolution of 110 nm under 20 times magnification.

## 2.4. Roughness Analysis

### 2.4.1. Surface Roughness Characterization

Each milled surface roughness is characterized according to the diagram presented in Figure 3 (Figure 3, Step B). Two dimensional (2D) and three dimensional (3D) roughnesses are computed according to ISO 4287, 4288 standards [25,26] for 2D roughness applications and ISO 25178 standards [28] for 3D applications. The 3D roughness parameters are computed on  $0.8 \times 1 \text{ mm}^2$  planar surfaces. Two surfaces per sample are recorded and 3D roughness are computed in the middle of the milled surface. Then, the mean and standard deviation are calculated. In accordance with standard EN 623-4 [29], aberrant points are excluded from the area, if necessary. From each 3D surface recording, 2D roughness profiles are selected and extracted perpendicularly to the feed rate direction (Figure 4a). Three profiles (around 1 mm length) per sample are selected in the middle of the milled surface. Then, the mean and standard deviation are calculated.

### 2.4.2. Surface Roughness Parameters

The observed 2D roughness parameters are Ra (average roughness of profile), Rt (maximum peak to valley height of roughness profile) and Rz (mean peak to valley height of roughness profile) [25–27]. The observed 3D roughness parameters are Sa (average height of selected area), Sz (maximum valley depth of selected area) and Sq (root-mean-square height of selected area) [28]. Ceramic surface roughness is recorded according to standard EN 623-4 [29].

### 2.4.3. Statistics

Sa and Ra roughness parameter data are extensively analysed by using Kruskal-Wallis (K-W) non-parametric analysis tests ( $\alpha = 0.05$ ).

## 3. Results

First, the six measured roughness parameters (Ra, Rt, Rz, Sa, Sq, Sz) and the recorded surface topology of the machined surfaces of the eight tool-biomaterial couples are determined. Then, according to the results, the relationship between the roughness parameters obtained and the hardness of the machined biomaterial is characterized. Afterwards, the impact of the feed rate on the roughness is defined and, finally, the K-W statistical tests results are taken into account.

### 3.1. Results of Surface Roughness Experiments

The surfaces of the eight tool-biomaterial couples observed, machined with the two LY and CER tools, showed isotropic surfaces without the presence of pronounced peaks and/or valleys (Figure 4). The roughness results obtained with the LY and CER tools are shown in Figures 5 and 6. The roughness parameters measured with the CER tool were very close to those obtained with the LY tool. We noted that the standard deviations (SD) were lowest for the Ra and Sa roughness parameters. Conversely, the highest SD were observed for the Rt, Rz, Sz, Sq roughness parameters. For both tools, the Ra parameters presented slightly higher values compared to the Sa values. Similarly, the Rt parameters were on average, four times higher than Sq. On the contrary, the 3D parameters Sz were four times higher on average, compared to the 2D Rz parameters.

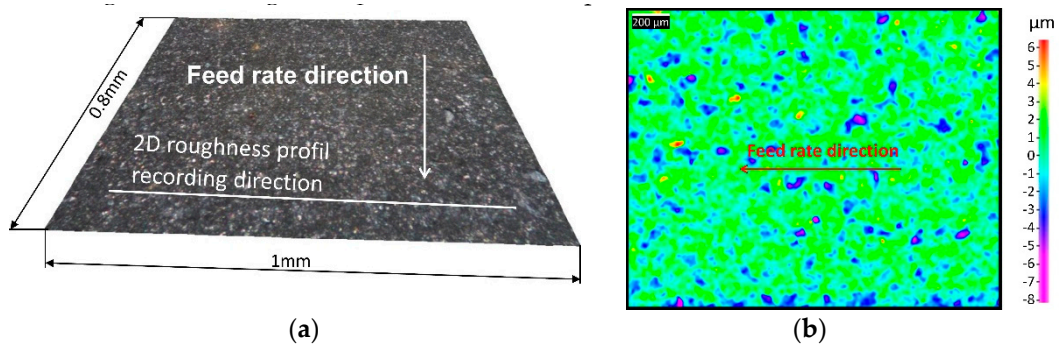


**Figure 4.** ENLY couple surface topology at a feed rate of 2000 mm/min. (a) 3D surface topology. (b) 3D surface roughness map.

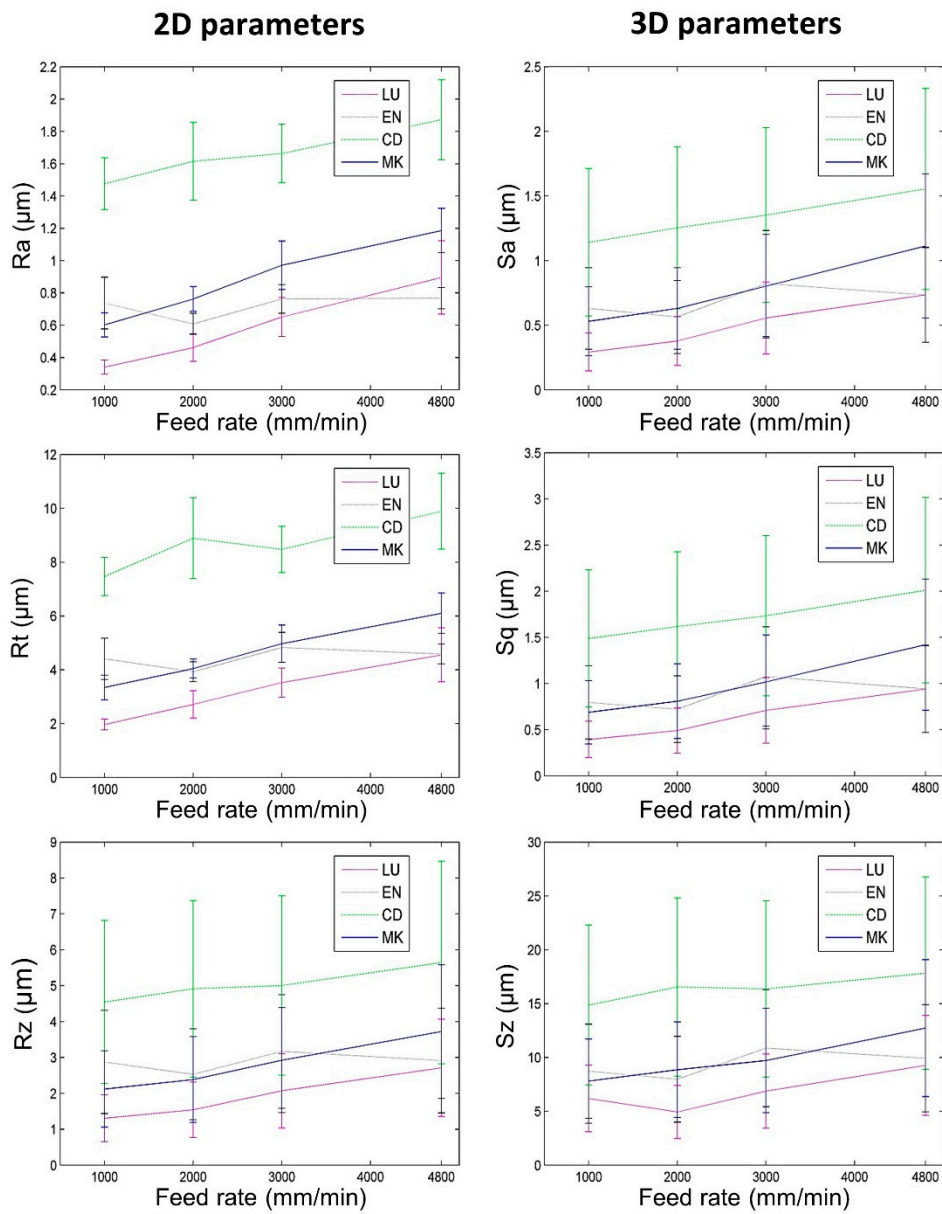


**Figure 5.** Roughness depending on prosthetic material and feed rates when milling with the Lyra tool (vertical bars represent standard deviation).

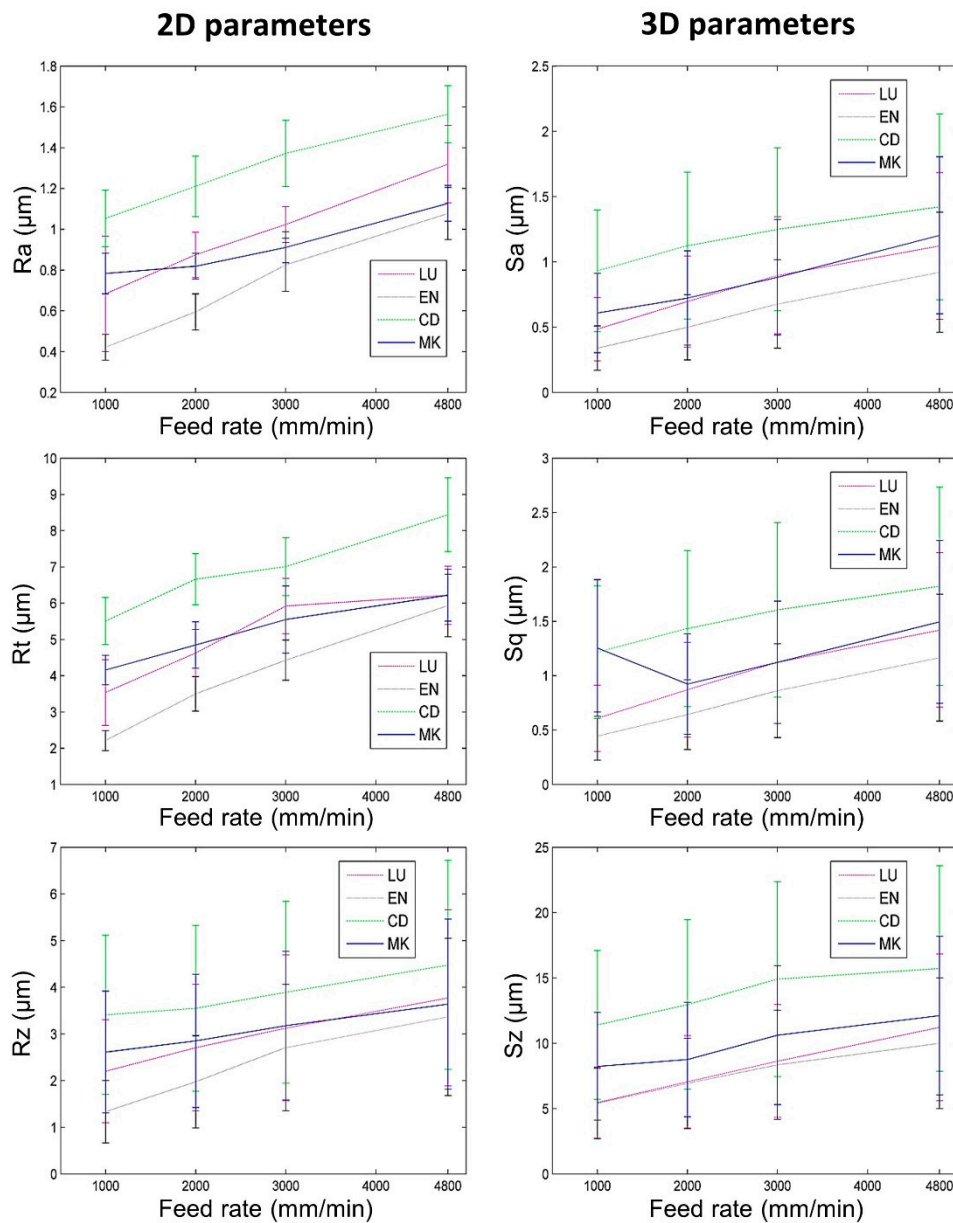


**Figure 6.** Roughness depending on prosthetic material and feed rate when milling with the Cerec tool (vertical bars represent standard deviation).

### 3.2. Surface Roughness vs. Biomaterial Hardness

For both tools (LY and CER) and all feed rates, the 2D and 3D surface roughnesses of biomaterials CD and MK (hardest biomaterials milled) were rougher than the other biomaterials (Figures 5 and 6). The roughness values of biomaterials LU and EN (milled soft and medium biomaterials) were the lowest. For each tool, the Ra and Sa roughnesses were observed to increase from the softest (LU) to the hardest (CD) biomaterial (Figure 7). The highest slope was observed between the medium (EN) and the hard (CD) biomaterials.



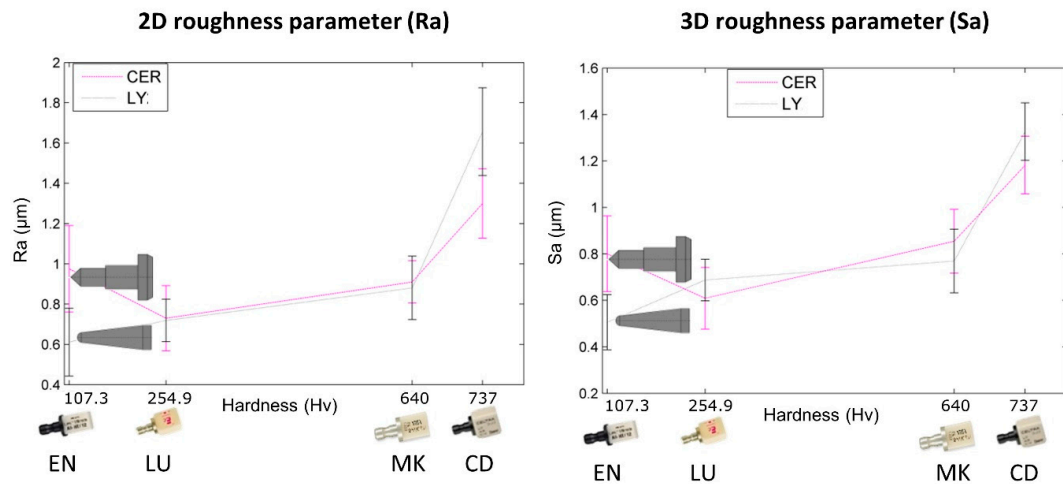


**Figure 7.** Correlations established between roughness and tool-biomaterial couples (vertical bars represent standard deviation).

### 3.3. Surface Roughness vs. Feed Rate

For the eight tool-biomaterial couples, it was observed that 2D and 3D surface roughness seemed to be weakly influenced by the feed rate (Figures 5 and 6). Regarding Ra and Sa, a mean increase of respectively 0.46  $\mu\text{m}$  and 0.48  $\mu\text{m}$  was observed when the feed rate ranged from 1000 to 4800 mm/min. Regarding Rz and Sz, a mean increase (1.23  $\mu\text{m}$  and 3.84  $\mu\text{m}$  respectively) was observed when the feed rate ranged from 1000 to 4800 mm/min. Sq increased by 0.54  $\mu\text{m}$ , and Rt increased by 2.42  $\mu\text{m}$ . Nevertheless, whatever the tool and the feed rate, the Sq parameters were equal or slightly higher than Sa.

### 3.4. Statistics

K-W pairwise correlations of Ra and Sa roughness parameter were obtained and the results are shown in Tables 4 and 5.

**Table 4.** Kruskal-Wallis statistical test results for Ra 2D roughness criterion.

Tool-Biomaterial Couples	LULY	LUCER	ENLY	ENCER	CDLY	CDCER	MKLY	MKCER
LULY								
LUCER	S *							
ENLY	NS **	S						
ENCER	S	NS	S					
CDLY	NS	S	NS	S				
CDCER	S	NS	S	NS	S			
MKLY	NS	S	S	S	NS	S		
MKCER	S	NS	S	NS	S	NS	S	

\* S: Significant, \*\* NS: Not Significant.

**Table 5.** Kruskal-Wallis statistical test results for Sa 3D roughness criterion.

Tool-Biomaterial Couples	LULY	LUCER	ENLY	ENCER	CDLY	CDCER	MKLY	MKCER
LULY								
LUCER	NS **							
ENLY	S *	S						
ENCER	S	NS	S					
CDLY	NS	S	NS	S				
CDCER	S	NS	S	NS	NS			
MKLY	NS	S	S	S	S	S		
MKCER	S	S	S	NS	S	NS	S	

\* S: Significant, \*\* NS: Not Significant.

Regarding the Ra roughness parameter, with only one exception (ENLY/MKLY), the K-W statistical tests revealed a significant difference in roughness for the same biomaterial machined with the two different tools. However, with only one exception (ENLY/MKLY), two different biomaterials machined with the same milling tool did not reveal any significant difference.

As for the Sa roughness parameter, with only two exceptions (LUCER/MKCER and ENLY/MKLY), the K-W statistical tests revealed a significant difference in roughness for the same biomaterial machined with the two different tools. However, with only two exceptions (LUCER/MKCER and ENLY/MKLY), two different biomaterials machined with the same milling tool did not reveal any significant difference.

#### 4. Discussion

The first null hypothesis that roughness does not vary depending on the tool-biomaterial couple is rejected. The second null hypothesis that roughness does not vary as a function of the feed rate is accepted.

In our study, six roughness parameters (Ra, Rt, Rz, Sa, Sq, Sz) are measured on eight tool-biomaterial couples.

End milling mode is currently used by a CNC chairside milling machine to manufacture the occlusal area (Figure 8), which plays a major role in many clinical functional requirements. Indeed, functional specifications such as wear, aesthetics, crack initiation, and prosthesis lifetime are located on the occlusal shape [30]. Antagonist tooth wear is impacted by the roughness of the occlusal prosthesis. Moreover, a rough surface led to poor light reflection and thus ultimately to an aesthetic defect. In addition, a rougher occlusal surface may promote crack initiation. Finally, rougher surfaces facilitate discoloration and decrease the resistance/lifetime of restoration. The clinical machining conditions are, in our study, replicated by machining a planar surface in end milling mode, with two advantages. (1) Roughness measurements are performed on milled planar surfaces, since roughness is not homogenous on complex/curved shapes and cannot be measured with trueness. (2) Reproduce the same CAD/CAM machining conditions as those used in a dental daily practice when milling the occlusal area.

Because the tool total milling time (92 s including the four feed rates) is shorter than its tool life, the same tool was used to experiment with the four feed rates (1000-2000-3000-4800 mm/min) [31].

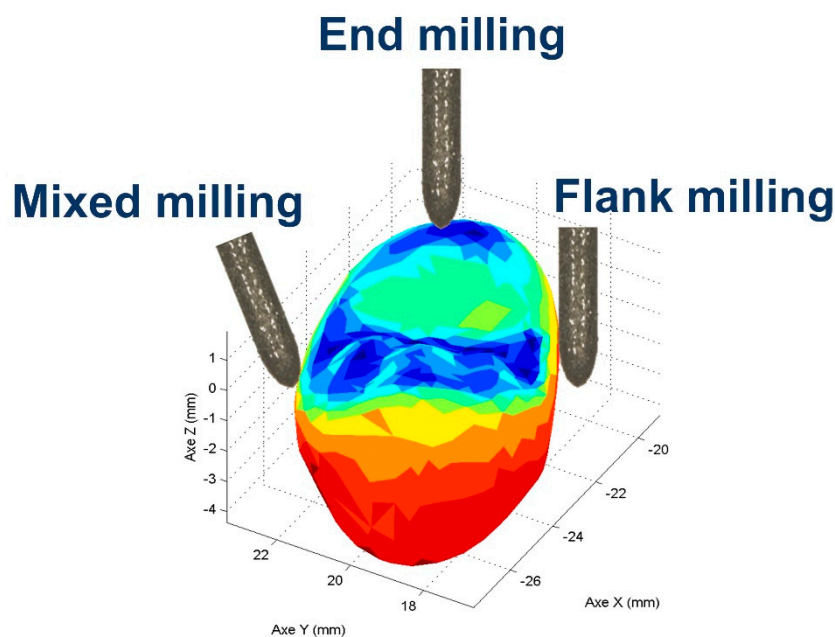


**Figure 8.** Tool milling mode applied on a dental crown, where the areas milled in end milling mode are in blue (occlusal shape) [30].

#### 4.1. Results of Surface Roughness Experiments

End milling with backwards and forwards sweeping (fifty in our case) using a ball-end tool tip and a constant radial depth ( $ar$ ) should leave an anisotropic surface signature. This anisotropic signature should be generated by the scallop leaves on the surface by the combination of the tool tip geometry and two consecutive sweeps (Figure 9). Nevertheless, the milled surface observations (Figure 4) revealed isotropic surface topologies on all the samples. The isotropic topology was confirmed by additional roughness measurements parallel to the feed rate direction. These results suggest that ball-end tool geometry is not a key parameter that impacts roughness in end milling mode and highlights the importance of the tool diamond grits not taken into account by the geometrical model proposed and described in Figure 9. In end milling mode, very few diamond grits are in contact with the machined surface and the tool wear is caused by a null cutting speed near the tool axis, increasing the pullout/wear of the grits. This phenomenon can explain the low roughness values observed on the milled surfaces with the two tools. The abrasive grains lost from the tool during milling can be displaced and compressed between the surface to be machined and the tool, causing three-body abrasion. The resulting phenomenon, called lapping [32], is consistent with our results and leads to low roughness parameters and an isotropic surface topology.

To summarize, the isotropic topology is left by the milling toolpath (backwards and forwards sweeping) associated with the lapping phenomena caused by diamond grits immersed in the coolant.

With both tools, the 3D parameters  $S_z$  are four times greater, on average, compared to the 2D  $R_z$  parameters. This can be explained by a larger number of extreme values found on surfaces than on linear profiles.

It was also noticed that the standard deviations (SD) were lower for the  $R_a$  and  $S_a$  parameters. The  $R_a$  and  $S_a$  parameters are based on an arithmetic mean, so extreme points have a limited influence on  $R_a$  and  $S_a$ .  $R_t$ ,  $R_z$ ,  $S_q$ , and  $S_z$  are extremum parameters. Due to the intrinsic definition/formula of these roughness parameters, giving a lot of weight to the maximum points,  $R_t$ ,  $R_z$ ,  $S_q$ , and  $S_z$  are very sensitive to these maximum values, which is why their SD values are higher.

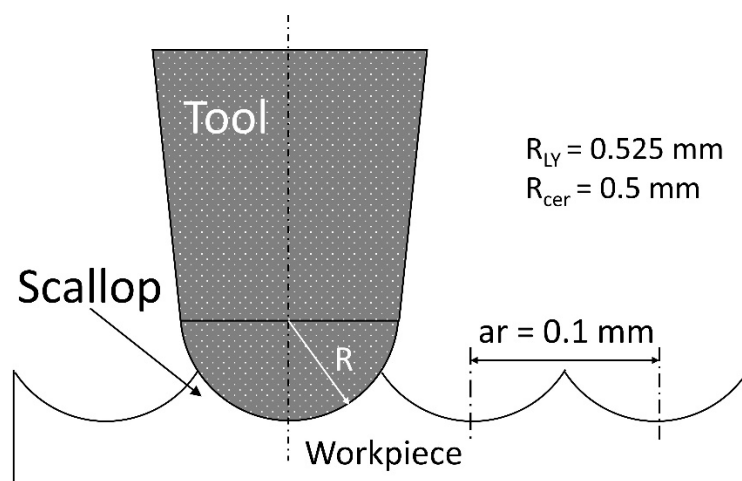


**Figure 9.** Geometric model of the 2D roughness obtained with the 2 tools tested in end milling mode.

#### 4.2. Surface Roughness vs. Biomaterial Hardness

It was observed that the roughness due to CD and MK surface were higher than those due to the LU and EN surface, whatever the tool used and the roughness parameter chosen. Although the milling mode and the machining parameters tested lacked a precise description in their article, Mota et al. also found that EN and LU biomaterials each exhibited a lower roughness than the others after milling [33].

In our study, Figure 7 shows that arithmetic roughness depends on the biomaterial's Vickers hardness ( $H_v$ ). In the range 107.3 (LU) to 254.9  $H_v$  (EN), arithmetic roughness parameters fluctuate,

and no trend can be found. Then, from 254.9 (EN) to 640 Hv (MK) a smooth roughness increase is observed. Finally, up to 737 Hv (CD) a more abrupt increase is observed. In conclusion, the arithmetic roughness is influenced by the biomaterial milled, more specifically its hardness.

#### 4.3. Surface Roughness vs. Feed Rate

For the eight tool-biomaterial couples, it was observed that the 2D and 3D roughness was weakly dependent on the feed rate in end milling, regardless of the standard deviation. The lapping phenomenon seemed to be dependent on the feed rate, thus explaining the slightly higher roughness parameters at high feed rates [34,35]. In these conditions, a higher feed rate seems to be a better solution to save manufacturing time, without significantly increasing roughness. Although the milling conditions tested were not representative of CAD/CAM milling, Chavali et al. in their article also found that opportunities may exist for exploring increased feed rates during the milling process when polymer-containing materials (Lava Ultimate and Enamic) are used in an effort to decrease milling times [36].

It was also noticed that for all the feed rates, the Sq 3D roughness parameters measured on surfaces were equal or slightly higher than the arithmetical average Sa 3D roughness. The 3D Sq parameter represents the standard deviation of roughness. From the point of view of the machined surfaces optical quality, it is better to have surfaces having a Sq equivalent to Sa. The Sq parameter gives more weight to the extremum values, a low Sq reveals the absence of significant peaks and valleys, sources of diffuse light reflection not revealed through the arithmetic Sa parameter.

#### 4.4. Statistics

For the eight tool-biomaterial couples tested and according to the definitions of the roughness parameters, we observed greater sensitivity of parameters Rt, Rz, Sz and Sq to extremum points. As a result, these roughness parameters exhibited higher mean values and higher standard deviations compared to Ra and Sa (arithmetic parameters). Hence, the K-W statistical tests ( $\alpha = 0.05$ ) were performed only on the arithmetic parameters Ra and Sa which were less sensitive to the extreme values. K-W pairwise correlations of the Ra and Sa roughness parameters were established (Tables 4 and 5).

Except for two Sa parameter statistical comparisons (LULY/LUCER, CDCER/CDLY), the K-W tests revealed the influence of the tool used in end milling mode on the Ra and Sa roughness parameters. This tool influence, not highlighted by the results of the surface roughness experiments (§4.1), was revealed by the K-W statistical tests. One Ra exception (ENLY/MKLY), and four Sa exceptions (ENLY/LULY, MKCER/LUCER, MKLY/ENLY, CDLY/MKLY) were observed. Each time these exceptions corresponded to different biomaterials machined with the same tool, thus confirming the secondary influence of the milled biomaterial on the roughness parameters during end milling.

To summarize, according to the Ra and Sa K-W statistical results, the tool has first an influence on the roughness obtained by end milling mode. The machined biomaterial secondly influences the roughness.

#### 4.5. Flank Milling Mode vs. End Milling Mode

A previous study [37] showed that higher roughness and anisotropic topology are generated in flank milling mode compared to the roughness and isotropic topology obtained in end milling mode. However, the flank milling mode is applied on the peripheric areas, while the end milling mode is applied on the occlusal areas. As a result, each area can be milled with the best tool-biomaterial couple able to satisfy the expected local functional specifications.

Although we observed surface topology and measured roughness on surfaces milled in end milling mode, other factors have to be considered for a more comprehensive assessment of the obtained surface integrity. In this regard, the impacts of the coolant and the tool wear were not taken into account in this study. Moreover, further measurements on curved surfaces known to facilitate roughness filtering should be undertaken.

## 5. Conclusions

The milling mode, the relative orientation between the axis of the diamond rotary cutting instruments and the prosthesis surface have a significant impact on surface integrity and more specifically on roughness. Several prosthesis surface requirements such as aesthetics, biological response (soft tissue response and plaque accumulation) and mechanical behavior are influenced by residual roughness after milling. Therefore, for each clinical requirement, a specific roughness can be manufactured with the appropriate milling mode.

Under the limitations of this study, the following conclusions can be drawn. The tool-material couple must be taken into account when the prosthesis surfaces are manufactured with the end milling mode. Indeed, the milled surface roughness is affected by the biomaterial's hardness. The roughness also depends on the tool, and less on the feed rate.

Our results suggest that the tool used in end milling mode must be chosen in correlation with the expected surface roughness and the dental biomaterial milled, which both obviously affect the integrity of the surface. High feed rates can be set to save manufacturing time, without significantly increasing roughness.

The lapping phenomenon seems to occur and generate low roughness parameters in end milling mode. According to our results, end milling mode is an obvious choice when producing a dental prosthesis for which low roughness is desired.

**Author Contributions:** Conceptualization, methodology, original draft preparation, must be acknowledged to N.L. Writing-review and editing must be acknowledged to E.V. Supervision must be acknowledged to L.T. All authors have read and agreed to the published version of the manuscript.

**Funding:** This research received no external funding.

**Acknowledgments:** The authors would like to thank Lyra-GACD for supporting this study with material.

**Conflicts of Interest:** The authors declare no conflict of interest.

## References

1. MarketWatch. Dental CAD/CAM Market Witness a Remarkable Growth at 8.1% CAGR Projected to Reach USD 3.33 Billion By 2027. Available online: <https://www.marketwatch.com/press-release/dental-cadcam-market-witness-a-remarkable-growth-at-81-cagr-projected-to-reach-usd-333-billion-by-2027-2019-02-08> (accessed on 25 February 2020).
2. Idata Research. *Europe Market Report Suite for Digital Dentistry*; iDATA\_EUDIGD18\_MS; iData Research Inc.: Burnaby, BC, Canada, 2018.
3. Idata Research. *US Market Report Suite for Digital Dentistry*; iDATA\_USDIGD18\_MS; iData Research Inc.: Burnaby, BC, Canada, 2018.
4. Jawahir, I.S.; Brinksmeier, E.; M'saoubi, R.; Aspinwall, D.K.; Outeiro, J.C.; Meyer, D.; Jayal, A.D. Surface integrity in material removal processes: Recent advances. *CIRP Ann.-Manuf. Technol.* **2011**, *60*, 603–626. [[CrossRef](#)]
5. Yin, L.; Song, X.F.; Qu, S.F.; Han, Y.G.; Wang, H. Surface integrity and removal mechanism in simulated dental finishing of a feldspathic porcelain. *J. Biomed. Mater. Res.* **2006**, *79*, 365–378. [[CrossRef](#)]
6. Sorensen, J.A. A rationale for comparison of plaque retaining properties of crown systems. *J. Prosthet. Dent.* **1989**, *62*, 264–269. [[CrossRef](#)]
7. Heintze, S.D. Crown pull-off test (crown retention test) to evaluate the bonding effectiveness of luting agents. *Dent. Mater.* **2010**, *26*, 193–206. [[CrossRef](#)]
8. Hickel, R.; Peschke, A.; Tyas, M.; Mjör, I.; Bayne, S.; Peters, M.; Hiller, K.A.; Randall, R.; Vanherle, G.; Heintze, S.D. FDI World Dental Federation: Clinical criteria for the evaluation of direct and indirect restorations-update and clinical examples. *J. Clin. Oral Investig.* **2010**, *14*, 349–366. [[CrossRef](#)] [[PubMed](#)]
9. Bollen, C.M.L.; Lambrechts, P.; Quirynen, M. Comparison of surface roughness of oral hard materials to the threshold surface roughness for bacterial plaque retention: A review of the literature. *Dent. Mater.* **1997**, *13*, 258–269. [[CrossRef](#)]

10. Heintze, S.; Forjanic, M.; Rousson, V. Surface roughness and gloss of dental materials as a function of force and polishing time in vitro. *Dent. Mater.* **2006**, *22*, 146–165. [[CrossRef](#)] [[PubMed](#)]
11. Mormann, W.H.; Stawarczyk, B.; Ender, A.; Sener, B.; Attin, T.; Mehl, A. Wear characteristics of current aesthetic dental restorative CAD/CAM materials: Two-body wear, gloss retention, roughness and Martens hardness. *J. Mech. Behav. Biomed. Mater.* **2013**, *20*, 113–125. [[CrossRef](#)] [[PubMed](#)]
12. Tuntiprawon, M. Effect of tooth surface roughness on marginal seating and retention of complete metal crowns. *J. Prosthet. Dent.* **1999**, *81*, 142–147. [[CrossRef](#)]
13. Li, Y.Q.; Wang, H.; Wang, Y.J.; Chen, J.H. Effect of different grit sizes of diamond rotary instruments for tooth preparation on the retention and adaptation of complete coverage restorations. *J. Prosthet. Dent.* **2012**, *107*, 86–93. [[CrossRef](#)]
14. Scurria, M.S.; Powers, J.M. Surface roughness of two polished ceramic materials. *J. Prosthet. Dent.* **1994**, *71*, 174–177. [[CrossRef](#)]
15. Gui, C.; Elwenspoek, M.; Tas, N.; Gardeniers, J.G.E. The effect of surface roughness on direct wafer bonding. *J. Appl. Phys.* **1999**, *85*, 7448–7454. [[CrossRef](#)]
16. Dirxen, C.; Blunck, U.; Preissner, S. Clinical Performance of a New Biomimetic Double Network Material. *Open Dent. J.* **2013**, *7*, 118–122. [[CrossRef](#)] [[PubMed](#)]
17. Zimmermann, M.; Mehl, A.; Reich, S. New CAD/CAM materials and blocks for chairside procedures. *Int. J. Comput. Dent.* **2013**, *16*, 173–181.
18. Facenda, J.C.; Borba, M.; Corazza, P.H. A literature review on the new polymer infiltrated ceramic network material (PICN). *J. Esthet. Restor. Dent.* **2018**, *30*, 281–286. [[CrossRef](#)]
19. Lambert, H.; Durand, J.C.; Jacquot, B.; Fages, M. Dental biomaterials for chairside CAD/CAM: State of the art. *J. Adv. Prosthodont.* **2017**, *9*, 486–495. [[CrossRef](#)]
20. Yin, L.; Huang, H. Ceramic response to high speed grinding. *Mach. Sci. Technol.* **2004**, *8*, 21–37. [[CrossRef](#)]
21. Hecker, R.L.; Liang, S.Y. Predictive modeling of surface roughness in grinding. *Int. J. Mach. Tool Manuf.* **2003**, *43*, 755–761. [[CrossRef](#)]
22. AFNOR. NF E 66-520-1 to 8. In *Working Zones of Cutting Tools—Couple Tool-Material*; AFNOR: La Plaine Saint Denis, France, 1997.
23. Taylor, F.W. On the art of cutting metal. *Trans. ASME* **1907**, *28*, 1–247.
24. Brinksmeier, E.; Klocke, F.; Lucca, D.A.; Sölter, J.; Meyer, D. Process Signatures—a new approach to solve the inverse surface integrity problem in machining processes. *Procedia CIRP* **2014**, *13*, 429–434. [[CrossRef](#)]
25. ISO. ISO-4287. *Geometrical Product Specifications (GPS)—Surface Texture: Profile Method—Terms, Definitions and Surface Texture Parameters*; ISO: Genève, Switzerland, 1998.
26. ISO. ISO-4288. *Geometrical Product Specifications (GPS). Surface Texture: Profile Method. Rules and Procedures for the Assessment of Surface Texture*; ISO: Genève, Switzerland, 1998.
27. ISO. ISO-12085. *Geometrical Product Specifications (GPS)—Surface Texture: Profile Method—Motif Parameters*; ISO: Genève, Switzerland, 1998.
28. ISO. ISO-25178-2. *Geometrical Product Specifications (GPS)—Surface Texture: Areal Part 2: Terms, Definitions and Surface Texture Parameters*; ISO: Genève, Switzerland, 2012.
29. ISO. EN-623-4. *Advanced Technical Ceramics—Monolithic Ceramics—General and Textural Properties—Part 4: Determination of Surface Roughness*; ISO: Genève, Switzerland, 2004.
30. Lebon, N.; Tapie, L.; Vennat, E.; Mawussi, B. A Computer-Aided Tool to Predict Dental Crown Prosthesis Surface Integrity after Milling. *Comput.-Aided Des. Appl.* **2019**, *16*, 894–903. [[CrossRef](#)]
31. Corazza, P.H.; Lago de Castro, H.; Feitosa, S.A.; Kimpara, E.T. Influence of CAD-CAM diamond bur deterioration on surface roughness and maximum failure load of Y-TZP-based restorations. *Am. J. Dent.* **2015**, *28*, 95–99. [[PubMed](#)]
32. Evans, C.J.; Paul, E.; Dornfeld, D.; Lucca, D.A.; Byrne, G.; Tricard, M.; Mullany, B.A. Material removal mechanisms in lapping and polishing. *CIRP Ann.-Manuf. Technol.* **2003**, *52*, 611–633. [[CrossRef](#)]
33. Mota, E.G.; Smidt, L.N.; Fracasso, L.M.; Burnett, L.H., Jr.; Spohr, A.M. The effect of milling and postmilling procedures on the surface roughness of CAD/CAM materials. *J. Esthet. Restor. Dent.* **2017**, *29*, 450–458. [[CrossRef](#)] [[PubMed](#)]
34. Buijs, M.; Korpel-van Houten, K. Three-body abrasion of brittle materials as studied by lapping. *Wear* **1993**, *166*, 237–245. [[CrossRef](#)]

35. Li, S.; Wang, Z.; Wu, Y. Relationship between subsurface damage and surface roughness of optical materials in grinding and lapping processes. *J. Mater. Process. Technol.* **2008**, *205*, 34–41. [[CrossRef](#)]
36. Chavali, R.; Nejat, A.H.; Lawson, N.C. Machinability of CAD-CAM materials. *J. Prosthet. Dent.* **2017**, *118*, 194–199. [[CrossRef](#)]
37. Lebon, N.; Tapie, L.; Vennat, E.; Mawussi, B. Influence of CAD/CAM tool and material on tool wear and roughness of dental prostheses after milling. *J. Prosthet. Dent.* **2015**, *114*, 236–247. [[CrossRef](#)]



© 2020 by the authors. Licensee MDPI, Basel, Switzerland. This article is an open access article distributed under the terms and conditions of the Creative Commons Attribution (CC BY) license (<http://creativecommons.org/licenses/by/4.0/>).